AUTOMATED COMBINED TECHNIQUE FOR SEGMENTING CYTOLOGICAL SPECIMEN IMAGES

D. M. Murashov
Computing Centre of the Russian Academy of Sciences, 40, Vavilov street, Moscow, GSP-1, 119991, Russia

Keywords: Segmentation technique, active contour, dynamic system, height ridges, wave equation, cytological images.

Abstract: Automated snake-based combined technique for segmenting cytological images is proposed. The main features of the technique are: implementation of the wave propagation model and modified Gaussian filter based on the heat equation with heat source, availability of coarse and precise levels of contour approximation, automated snake initiation. The technique is successfully implemented for segmenting cytological specimen images.

1 INTRODUCTION

One of the problems arising in the field of automated diagnostics of hematological diseases is the segmentation of nuclei in the cytological specimen images for subsequent calculation of diagnostic features. It is necessary to obtain such a closed curve in the specimen image that follows the boundary of selected nucleus with an adequate accuracy.

Haralick and Shapiro (Haralick and Shapiro, 1985) established the following requirements to images leading to successful segmentation: homogeneousness of regions in image with respect to some characteristics; topological simplicity, significant difference of characteristics of adjacent regions; simplicity, smoothness, and spatial accuracy of region boundaries.

An image of a lymphoid tissue stained by Romanovski-Giemsa technique is a color image (24 bpp) taken by a camera mounted on Leica DMRB microscope using PlanApo 100/1.3 objective. The equivalent size of a pixel was 0,0036 μ^2. Cytological specimen images have the following specific features plaguing the solution. Firstly, because of poor dye quality the boundary between cytoplasm and a cell nucleus may be indistinctive. Secondly, cells may be located closely to each other, in part may be overlapped. Thirdly, adjacent nuclei may have more strong boundaries, than selected nucleus. Fourthly, strong edges reflecting chromatin structure inside the nucleus appear.

Due to the features listed above any single technique failes to solve the segmentation task properly (Bengtsson, 2004). Currently the researches more often turn their attention to combined techniqes.

A combined technique for automated segmenting of cell nuclei in cytological specimen images is proposed. The solution of segmentation problem is obtained by combining two level active contour model and thresholding procedure with automatically estimating thresold value from image histogram in CIE *Lab* colour space.

Two level active contour model (or snake) is formed using nonlinear model of a dynamic system in terms of state-space. A snake can be initiated in automated and manual modes. Taking into account the properties of the stain, segmentation at a coarse level is operating using blue colour component in RGB space. Correction at precise level of segmentation is made using the green component. To eliminate the influence of the neighboring nuclei boundaries the modified Gaussian filter based on the heat equation with a heat source is used. In order to increase the capture range of the snake the wave propagation model is implemented.

2 METHODS FOR SEGMENTING SPECIMEN IMAGES

One of the popular segmentation techniques in cytology is thresholding with automatically estimated threshold value (Borst, 1979). The technique is computationally simple but it is effective only in case when objects and background differ in colour or

M. Murashov D. (2007).
AUTOMATED COMBINED TECHNIQUE FOR SEGMENTING CYTOLOGICAL SPECIMEN IMAGES.
In *Proceedings of the Second International Conference on Computer Vision Theory and Applications*, pages 238-245
DOI: 10.5220/0002071402380245

gray level. In more complicated cases the segmentation consists in extraction of features per pixel and their classification into different classes of subregions. But in many cases the segmentation should be controlled and the result should be corrected interactively.

Using the simple techniques, one may run into problems if the nuclei are clustered, the image background is inhomogeneous, and there are intensity variations within the nuclei. By combining the methods some of these problems can be solved. For segmentation of cell nuclei in histological tissue images, the method based on watersheds and distance transform (Malpica, 1997) was proposed. In (Bengtsson, 2004), a method for segmentation of cell nuclei in tissue images by combining seeded watersheds with gradient and shape information was presented. The main disadvantage of these methods is that one should have a tool for correcting the results manually in complicated cases. In (Comaniciu, 2001) an approach based on nonparametric clusterization using gradient ascent mean shift procedure is presented. The algorithm outlines clusters in *Luv* space and marking their boundaries. But for obtaining the suitable result the manual merging of clusters is needed. In (Colantonio, 2006) a pixel-by-pixel nural network classification procedure is presented. The network is trained using clustering algorithm. The procedure is efficient but a special tool for correcting the results manually in difficult cases is needed.

For segmentation of cell nuclei in histological and cytological images, active contour models (parametric and geometric), or snakes, were used in (Klemencic, 1998, Ortiz de Solorzano, 2001, Leymarie, 1990). Snakes provide the smooth contour without gaps at the object boundary. Snakes were firstly proposed in (Kass, 1987). The main idea of parametric active contours is the following. Parametric active contour is defined as a curve $v(s) = [x(s), y(s)], s \in [0,1]$ (here, s is a parameter), that moves through the spatial domain of an image minimizing the energy functional:

$$E = \int_s \left[(1/2)\left(\alpha |v'(s)|^2 + \beta |v''(s)|^2 \right) + E_{ext}(v(s)) \right] ds \quad (1)$$

where $v'(s)$ and $v''(s)$ (the first and the second derivatives of $v(s)$ with respect to s) characterize the energy of internal forces, α and β are weighting parameters that controls snake's tension and rigidity, E_{ext} – the energy of the external force. The external force pulls the snake toward the object boundaries. The functional (1) achieves its minimum at the boundaries of the object. A gray-level image $I(x, y)$ is considered as a function of spatial coordinate variables (x, y). E_{ext} is defined as:

$$E_{ext}(x, y) = -\left| \nabla \left[G_\sigma(x, y) * I(x, y) \right] \right|^2 \quad (2)$$

where $G_\sigma(x, y)$ denotes the a Gaussian kernel with standard deviation σ, ∇ denotes the gradient operator, * denotes the convolution. As σ increases, the blurring appears and the capture range of the active contour increases. The curve that minimizes (1, 2) must satisfy the Euler equation. A numerical solution of the equation can be found using an iterative procedure which is finished when the balance of forces is achieved. The main disadvantage of the method is the limited capture range. The effective solution of this problem is the Gradient Vector Flow (GVF) method, proposed in (Xu, 1998). Within this framework, a new external force which is the solution of the generalized diffusion equation is used. This force minimizes the new energy functional that includes the term compensating the lack of force farther away from the object boundaries. Such a model increases the capture range and provides convergence to boundary concavities, but it is computationally expensive. Geometric active contours (Caselles, 1993) are based on the curve evolution theory and level set method. This model is less computationally expensive than parametric model and makes it possible to segment more than one object in the image. The model provides good results for images with high contrast. When the object boundary has gaps, the contour leaks through the boundary. A modified model, based on the relation between active contours and the computation of geodesics in a Riemannian space (Sapiro, 2001), eliminates leaking at some extent. In (Yang, 2005) authors proposed a combined snake-based approach to segmentation of tissue images using colour gradients in *Luv* space. For snake initializing a classifier is used. Classifier is trained using sample images selected by experts.

Thus, one may conclude that: (a) the task of development fully automated segmentation technique is actual; (b) only combined techniques can provide the suitable result; (c) snakes are efficient for segmenting cell nuclei images and can be used in automated tools (d) snakes also provide within the same framework an instrument for manual segmentation in difficult cases. In the next sections the problems concerned with the development of automated combined snake-based technique are considered.

3 ACTIVE CONTOUR MODEL

For developing a segmentation technique it is necessary to have a model of the object boundary.

3.1 Boundary Model

In literature an object boundary is defined as an arrangement of local edges. Local edges are defined as discontinuities in image luminance from one level to another (Pratt, 2001). Various types of edge models are known (Rohr, 2001). In (Belyaev, 1998, Eberly, 1994) edges are defind in terms of surface theory as a ridge of the surface produced by the function of the gray-level gradient module computed from the image. In (Eberly, 1994) definitions of ridges are given in terms of extremal intencity values, in terms of principal curvature extremal values, and in terms of level surface. In this work the following definition of ridges is used (Eberly, 1994).

Let function $h(x): R^n \to R$ is of the class C^2.

Definition. Define $W = -H(h)$, where $H(h)$ is Hessian matrix, and let λ_i and v_i, $1 \le i \le n$ be its eigenvalues and eigenvectors. Assume that $\lambda_1 \ge ... \ge \lambda_n$ and $1 \le d \le n$. A point x is a ridge point of type *n-d* if $\lambda_d(x) > 0$ and x is a generalized maximum point of type *n-d* for h with respect to $V = [v_1, ..., v_d]$.

The function $h(x)$ has a generalized maximum of type *n-d* at x if $V^T \nabla h(x) = 0$ and $V^T H(h(x)) V$ is negative definite (Eberly, 1994).

Since $V^T H(h) V = diag\{\lambda_1 |v_i|^2, ..., \lambda_d |v_d|^2\}$ and the eigenvalues are ordered, the test for the ridge point reduces to $V^T \nabla h(x) = 0$ and $\lambda_d > 0$.

Let the gray image be described by the function $u(\boldsymbol{x}) \in C^3$, $u(\boldsymbol{x}): R^2 \to R^+$, $\boldsymbol{x}=(x,y)^T$. The coordinate frame *Oxyz* is introduced; the plane *Oxy* is coincident with the image plain, and $z=u(x,y)$. Let us consider the function $h(\boldsymbol{x}): R^2 \to R^+$,

$$h(\boldsymbol{x}) = \left|\nabla u(\boldsymbol{x})\right| = \sqrt{u_x^2 + u_y^2}\,, \qquad (3)$$

where $u_x = \frac{\partial u}{\partial x}$, $u_y = \frac{\partial u}{\partial y}$. In this case the ridge of the surface $h(x,y)$ will be a connected set of generalized maximum points of type 1 on the surface $h(x,y)$, vector v will be aligned with the surface principal direction orthogonal to the ridge direction at this point. For 2D images the following property follows from the ridge definition (from the condition of 1-maximum).

Property. At the ridge point of the surface $h(x,y)$ at least one principal direction is parallel to the coordinate plane *Oxy*.

We consider an object in the image as a connected set of points in some closed region $X \subset R^2$.

We consider an edge in the image $u=u(x,y)$ as a projection of $z = h(x, y)$ ridge onto *Oxy* plane.

We consider the boundary of an object in the image as a simple closed curve which includes the edges separating the inner object regions from the surrounding regions.

In the next section using the definitions and notions given here, an active contour model will be developed.

3.2 Active Contour Model

As the digital image includes a finite number of pixels, it is valid to present an active contour as a set of *n* dynamic pointwise objects:

$$\dot{x}(t) = f(x(t)),\ x(0) = x_0\,, \qquad (4)$$

where $\boldsymbol{x}=(x,y)^T$ is the vector of spatial coordinates, t is time. Function $f(\boldsymbol{x}(t)) \in C^2$ in the neighborhood of the edge points $\boldsymbol{x}_e$ should force the system (4) to move towards $\boldsymbol{x}_e$ and should provide stability with respect to $\boldsymbol{x}_e$. As soon as we consider a set of points modelling a continuous curve it is reasonable to say about stability only along the normal to the contour (or along the normal to the intensity edge).

Let us consider the function $h(x,y)$ (3). The function $z=h(x,y)$ defines the surface $V^2 \subset R^3$. Further on, we shall analyze the properties of the surface $z=h(x,y)$ in the neighborhood of points located at the intensity edge.

Statement. If the function in the right-hand part of the system (4) is constructed as $f = (h_x, h_y)^T$, the system (4) will be stable in the neighborhood of intensity edge in the sense of the first Lyapunov method (Lee and Markus, 1971):

$$f(x_e) = 0,\ \ \mathrm{Re}\,\lambda\left[f_x(x)\right]\big|_{x=x_e} < 0\,, \qquad (5)$$

where $f_x(x)\big|_{x=x_e}$ is a matrix of the linear approximation of the system (4) at $x=x_e$.

Proof. The linear approximation of the system (4) in the neighborhood of the edge point is described by the equation:

$$\begin{pmatrix} \dot{x} \\ \dot{y} \end{pmatrix} = \begin{pmatrix} h_{xx} & h_{xy} \\ h_{xy} & h_{yy} \end{pmatrix} \begin{pmatrix} x \\ y \end{pmatrix}. \qquad (6)$$

Here the system matrix is Hessian matrix. Let $O`x`y`z`$ be a coordinate frame with the origin at the *h(x,y)* ridge point *P* which is projected to the edge

point x_e in the *Oxy* plane, the axis *z`* is aligned with the surface normal, the axes *O`x`* and *O`y`* are aligned with the principal directions (it is assumed, that the couple of quadratic forms has different eigenvalues). We place the origin of the frame *Oxyz* in *P*. Let axis *Ox* align with the principal direction orthogonal to the ridge direction. The local surface structure in the neighborhood of $P \in V^2$ is determined by its Gaussian curvature

$$K(P) = \lambda_1\lambda_2 = (h_{x'x'}h_{y'y'} - h^2_{x'y'})/(1 + h^2_{x'} + h^2_{y'})^2,$$

where λ_1, λ_2 are the eigenvalues of matrix $I^{-1}II$, *I* and *II* are matrices of the first and the second fundamental quadratic forms. Gaussian curvature sign is the same as one of Hessian matrix determinant.

The following cases are considered.

1. *O`x`y`* plane is tangent to $h(x,y)$ surface and coinsides with *Oxy*. In this case $h_{x'} = 0$ and $h_{y'} = 0$, $h_{x'y'} = h_{y'x'} = 0$. If *P* is the local maximum, then $\lambda_1 < 0$, $\lambda_2 < 0$. The system (6) splits into two independent equations. In this case, the system matrix is the Hessian matrix, and its eigenvalues are equal to the principal curvatures λ_1, λ_2 of $h(x,y)$ at the point *P*. Hence, the system is stable according to the first Lyapunov method.

2. *O`x`y`* plane is tangent to $h(x,y)$ surface and coinsides with *Oxy* plane, $h_{x'y'} = h_{y'x'} = 0$, $\lambda_1 = h_{x'x'}$, $\lambda_2 = h_{y'y'}$. The *O`x`y`* plane is tangent to the surface and parallel to the *Oxy* plane. In this case $h_{x'} = 0$ and $h_{y'} = 0$. Let us assume $\lambda_1 < 0$, $\lambda_2 = 0$ (or $\lambda_1 = 0$, $\lambda_2 < 0$). Then the system will be stable in the sense of the first Lyapunov method along the *Ox* axis and neutral along the *Oy* axis. So, an object (4) will move from some initial point (x_0,y_0) to a point (0,y_0).

3. *O`x`y`* plane is tangent to $h(x,y)$ surface and coinsides with *Oxy* plane, $h_x = h_{x'} = 0$, and $h_y = h_{y'} = 0$; $\lambda_1 < 0$, $\lambda_2 > 0$, or vise versa. In this case, *P* is a saddle point, and the system is stable along one of the principal directions and tends to the closest local maximum along another one. So, at the steady state the pointwise objects move permanently along the curvature lines from the $h(x,y)$ saddle points towards the nearest local maxima or parabolic points. Hence, the snake is stable with respect to the intensity edge.

4. *O`x`y`* plane is tangent to $h(x,y)$ surface but does not coinside with *Oxy* (see Figure 1). According to the property of ridge points, at least one of the prncipal directions is parallel to image plane. Let axis *O`x`* be in *Oxy* plane. Axis *O`x* coinsides with *Ox`* and *Oy* axis directed along the projection of *O`y`* axis onto *Oxy* plane. In *O`x`y`z`* frame the surface will be described by a function

$$z' = \varphi(x', y'). \quad (7)$$

We shall find out how the Hessian matrix and its eigenvalues will change in *Oxyz* frame. Coordinates *x`*, *y`*, *z`* are transformed to coordinates *x*, *y*, *z* according to the following expression:

$$\begin{bmatrix} x \\ y \\ z \end{bmatrix} = \begin{pmatrix} 1 & 0 & 0 \\ 0 & \cos\theta & \sin\theta \\ 0 & -\sin\theta & \cos\theta \end{pmatrix} \begin{bmatrix} x' \\ y' \\ z' \end{bmatrix}, \quad -\frac{\pi}{2} < \theta < \frac{\pi}{2}.$$

Taking into account that $\varphi_{x'} = 0$ and $\varphi_{y'} = 0$ it is shown that the elemets of the Hessian matrix will be as follows:

$$\frac{\partial^2 z}{\partial x^2} = \frac{\varphi_{x'x'}}{\cos\theta}, \quad \frac{\partial^2 z}{\partial x \partial y} = 0, \quad \frac{\partial^2 z}{\partial y^2} = \frac{\varphi_{y'y'}}{\cos^3\theta}. \quad (8)$$

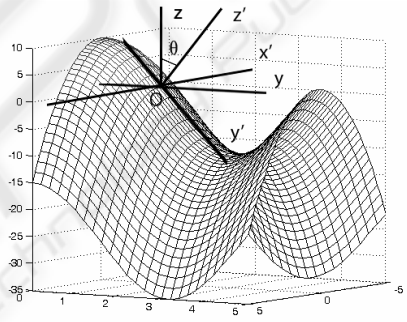

Figure 1: The surface *z=h(x,y)* and coordinate frames.

From (8) follows that theHessian is the diagonal matrix and the signs of the eigenvalues depend on *cosθ* sign. The expressions (8) can be justified by comparing formulas for Gaussian and mean curvature in both coordinate frames. Hence, as in cases described above, the linear approximation of the system (4) splits into two independent equations with respect to variables *x* and *y*. According to the conditions (5) the sysytem (4) will be stable with rspect to intensity edge. The statement is proofed.

In practice, the function in the right-hand part of the system (4) may be composed of several components. The main component f_0 is formed as a smoothed image edge map:

$$f_0(x) = \nabla[G_\sigma(x) * h(x)],$$

where $x=(x,y)^T$, *G* is the Gaussian kernel with standard deviation σ, ∇ is the gradient operator. The appearance of $f_0(x)$ for 1-D case and the stages of forming are shown in Figure 2 (a). Also, a smoothing term of the form $k_1 f_1(x)/|f_{\max}|$ (here $f_1(x)$ char-

acterizing the curvature, $f_{\max}$ is the maximum value of $f_0(x)$) is introduced in (4). Let $C(s) = (x(s), y(s))^T$ be a parameterized representation of the contour at fixed instant of time *t*, here, *s* - is the Euclidian arc length. We define $f_1(x)$ by the expression:

$$f_1(x) = C_{ss}(s),\ C_{ss}(s) = \left(\frac{d^2x}{ds^2}, \frac{d^2y}{ds^2} \right)^T .$$

Thus, the equation describing the dynamics of the pointwise object will be as follows:

$$\dot{x}(t) = f_0(x) / |f_{\max}| + k_1 f_1(x) / |f_{\max}|, \quad (9)$$

Coefficient k_1 is calculated from the stability conditions of model (9). To eliminate discontinuities and redundant contour points during evolution, resampling procedure is applied. For segmenting images with low contrast boundaries of the objects of interest and high contrast boundaries of adjacent objects, the two-level algorithm is proposed. At the first level, the coarse approximation of the boundaries is obtained. At the second level, the contour evolution results in precise boundary approximation.The initial condition of model (9) at the first level is the given initial contour, for example, an elipse. Initial condition at the second level is the contour obtained at the first level. The accuracy of segmentation substantially depends on nucleus edge map quality. At the first level, where the main goal of preprocessing is the obtaining of coarse nucleus edge map and suppression of high contrast edges of adjacent nuclei, the blue component of the input image is used. At the second level, where contour evolution results in precise boundary approximation, the influence of adjacent nuclei is not crucial, but it is necessary to operate with more precise and strong nucleus edge map. In this case, color reduction is performed by subtracting the green component from the input image.

3.3 Expanding the Capture Range

Within the developed technique, thresholding and subsequent Gaussian blurring are applied to the function $h(x,y)$ in order to strengthen and to level off the edge map. The standard deviation σ determines the capture range of the model (4). At large σ, the boundaries of the objects in the analyzed image disappear and the adjacent objects merge. The presented model accurately segments the objects of simple shapes with smooth boundaries. But it fails to segment the images with boundary concavities. Xu and Prince (Xu and Prince, 1998) proposed the GVF model that uses the vector field to force the snake to move. The vector field is computed from the image as the steady-state solution of a pair of linear partial differential equations. The GVF model provides the ability to move the snake into boundary concavities but it is computationally expensive. In this paper, in order to expand the capture range of the model (4), the model of wave propagation is used. The main idea is to spread the large values of the function in the right-hand part of (4) (see Figure 2 (b)).

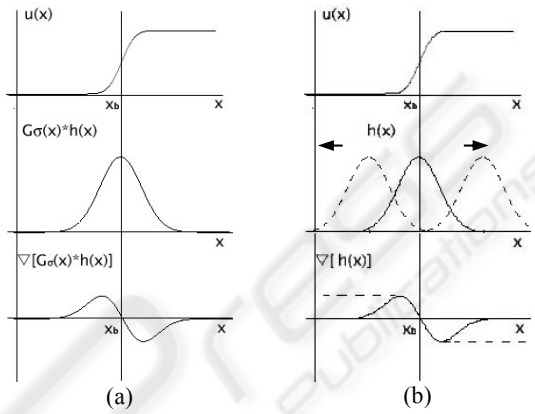

Figure 2: Constructing active contour model: (a) forming component $f_0(x)$ for 1-D case, top – object boundary, middle – smoothed edge map, bottom – function $f_0(x)$; (b) expanding the capture range of the active contour model.

Unlike the GVF model, there is no need to obtain the steady-state solution of differential equations. For this model, the Cauchy problem for the hyperbolic partial differential equation is solved with the initial conditions $w = G_\sigma h(x,y)$, $w_t = 0$:

$$\begin{aligned} &w_{tt}(x,y,t) = a^2 \Delta w(x,y,t), \\ &w(t_0) = G_\sigma h(x,y),\ \Delta = \partial^2/\partial x^2 + \partial^2/\partial y^2, \end{aligned} \quad (10)$$

where G_σ is the Gaussian kernel with standard deviation σ. Equation (10) describes the wave propagation process generated by the smoothed edge map. When solving equation (10) at each instant of time *t* at a point (*x,y*) the values of w_x, w_y are calculated, and maximal absolute values at the wave front are stored. The sign of the stored value is the same as the sign of the first nonzero value of w_x, w_y calculated at this point. Thus, the maximal gradient values of the function $G_\sigma h(x,y)$ propagate inside and outside the object boundary in natural way. The size of this region is defined by the value of *at*. In result, the vector field that forms the right hand part of model (4) is obtained. In Figure 3 (a)-(e) an example of segmenting of an object with non-convex boundary is shown: (a) – initial contour approximation, (b) – smoothed edge map, (c) and (d) - w_x, w_y, (e) – re-

sulting contour, bright regions correspond to positive values, dark ones – to non-positive values. The frame origin is at the top left corner of the image. In Figure 3 (f)-(k) the results of cell nucleus segmentation are shown: (f) – the initial contour approximation; (g) – coarse approximation; (h) – precise approximation, (i) – blurred edge map $G_\sigma h(x,y)$; (j), (k) – w_x, w_y at the second level.

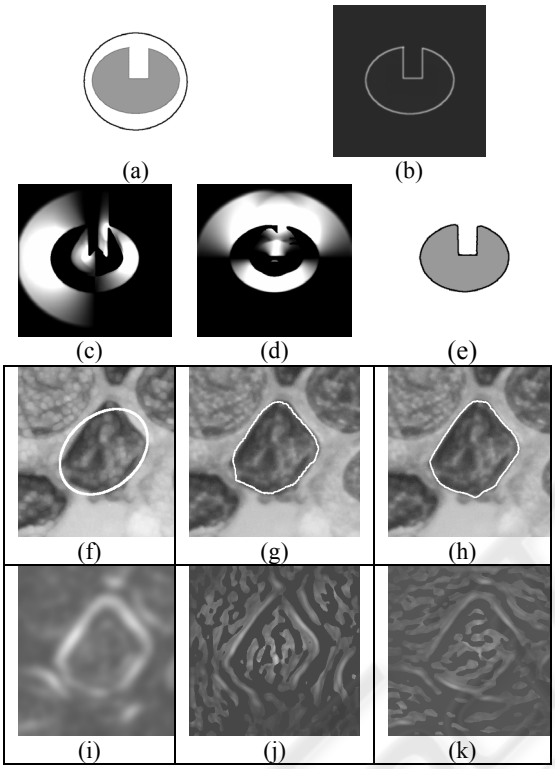

Figure 3: Image segmentation process: (a) – (e) – artificial image, (f) - (k) – cytological image.

3.4 Modified Gaussian Filter

For the successful operating of the active contour model two problems should be solved. Firstly, strong edges at the boundaries of the segmented nucleus should be obtained. Secondly, strong edges at the boundaries of the adjacent nuclei should be suppressed. For constructing function $f_0(x)$ in the right-hand part of the active contour model (9) Gaussian blur is used for image smoothing before obtaining the edge map $h(x)$ and then for blurring $h(x)$.

For suppressing strong edges at the boundaries of adjacent nucleus the modified Gaussian filter was applied. The Gaussian kernel used in a standard Gaussian filter is the fundamental solution of a heat equation (Koederink, J., 1984). The modified filter is constructed on the basis of a heat equation which features the development of two-dimensional non-stationary process in the fixed environment with heat sources or sinks:

$$u_t = u_{xx} + u_{yy} - F(x,y,t),\ \ u(t_0) = u_0,\ \ t_0 \le t \le t_f, \qquad (11)$$

here, $u = u(x,y,t)$ is the image under processing, x, y - are the spatial coordinates, t is time, t_0, t_f are initial and final moments. On the one hand, for image smoothing before obtaining edge map, the function $F(x,y,t)$ describing a source or sink of heat, should be designed so that the adjacent nuclei should not be smoothed and merge with one of interest. On the other hand, the function $F(x,y,t)$ should not generate the strong edges in the image edge map. Thus, we may define this function as follows:

$$F(x,y,t) = \begin{cases} u_{xx} + u_{yy}, (x,y) \notin \text{int}(C_0); \\ 0, (x,y) \in \text{int}(C_0), \end{cases} \qquad (12)$$

where $\text{int}(C_0)$ denotes the set of points (x,y) inside the initial approximation of contour C_0.For blurring the edge map the function $F(x,y,t)$ should be created so that it should essentially reduce the intensity of the pixels outside the initial contour C_0. For example, the function may be defined as follows:

$$F(x,y,t) = G_\sigma * \text{C}[FILL[\delta_B(C_0)]], \qquad (13)$$

for $t_0 \le t \le t_f$, where C_0 denotes the initial contour, δ_B denotes the dilation operator with the structuring element *B, FILL* denotes the fillhole operator (Soille, 2004), G_σ is the Gaussian kernel with standard deviation σ, * denotes the convolution, and C denotes the complementation operator. The size of structuring element B is set equal to σ. The initial approximation of the contour in this case should be set outside of the selected nucleus. In Figure 5 the stages of constructing the function $f_0(x)$ in the right-hand part of model (9) using the modified Gaussian filter with different functions $F(x,y,t_0)$ are illustrated. In Figure 4 (a) the given fragment of the preparation image with the initial contour C_0 is shown. In Figure 4 (b) $F(x,y,t_0)$ is shown. Figure 4 (c) the result of the initial image blurring with function $F(x,y,t_0)$ defined by (12) is presented. In Figure 4 (d) one can see the edge map obtained from the image in Figure 4 (c). In Figure 4 (e) the result of applying morphological opening and thresholding operations to the image in Figure 4 (d) is shown. In Figure 4 (f) the blurred image Figure 4 (e) is presented, here the function $F(x,y,t_0)$ is defined by expression (13). The scheme for the numerical solution of the equa-

tion (11) is based on the scheme presented in (Lindeberg, 1994).

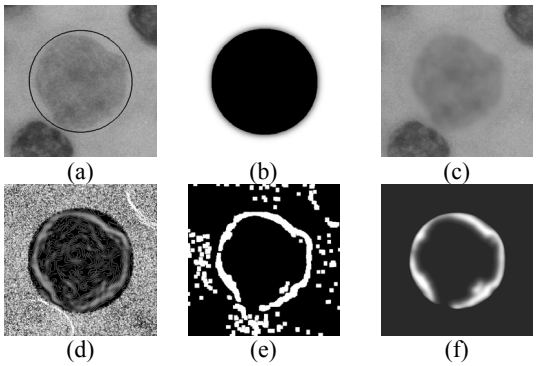

Figure 4: The stages of constructing the function $f_0(x)$ using modified Gaussian filter: (a) the given fragment of the preparation image and initial contour C_0 ; (b) the heat source function $F(x,y,t_0)$; (c) blurred image (a), the function $F(x,y,t_0)$ is defined as (12); (d) the edge map obtained from image (c); (e) the result of applying morphological opening and thresholding operations to image (d); (f) blurred image (e), the function $F(x,y,t_0)$ is defined as (13).

4 AUTOMATED SNAKE INITIALIZATION

In cytological specimen image segmentation tasks a lot of objects appeared in the image (see Figure 5) should be segmented.

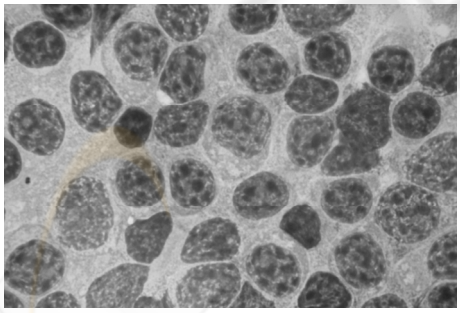

Figure 5: Cytological specimen image.

The manual snake initialization making segmentation task crucially time consuming. In (Yang, 2005) a classifier trained by example provided by experts is applied for obtaining rough approximation of objects used for initializing GVF snake. Taking into account instability of staining properties and conditions of specimen image aquizition the experts should train the classifier regularly.

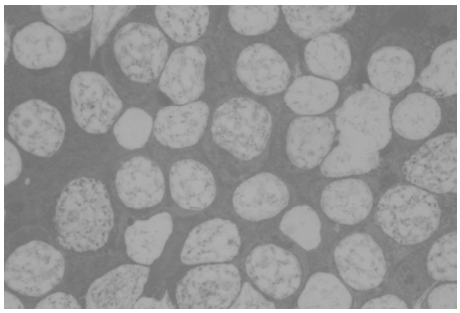

Figure 6: Component *a* of the specimen image in the CIE *Lab* color space.

In this work a simple automated initialization procedure based on the specimen staining properties is proposed. The procedure is based on the properties of specimens stained by Romanovsky-Giemza technique. Specimen image component *a* in the CIE *Lab* colour space (see Figure 6) has bimodal intensity histogram (see Figure 7).

Figure 7: Histogram of the image shown in Figure 6.

Using thresholding operation with automatic estimated threshold value one can obtain a binary mask of the specimen image (see Figure 8).

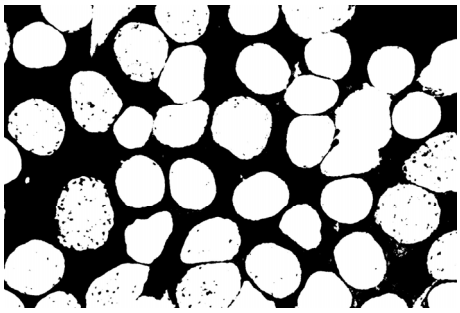

Figure 8: Binary mask of the image shown in Figure 7.

Further on, the following operations should be applied to each of the objects taken one-by-one in the binary mask image to obtain the corresponding initial approximation of the contour. First, morphological fillhole operation. Second, filtering by area value. Small objects are excluded. If the object area is large, an iterative procedure is applied to component *a* image fragment in order to find the threshold value at which the binary object splits into parts. After that, filtering is applied to each part of the ini-

tial object. Third, the white top-hat operation is applied to obtain contour initial approximation.

It is necessary to note, that at step 2 one may use distance transform operation to separate two touching objects instead of described iterative procedure. The iterative procedure is effective because of smoothness of intensity histogram.

5 CONCLUSIONS

The combined technique for automated segmenting of cell nuclei in cytological specimen images is proposed. The solution of segmentation problem is obtained by combining two level active contour model and thresholding procedure with automatically estimating threshold value from image histogram in CIE *Lab* colour space. The main features of the technique are: implementation of the wave propagation model and modified Gaussian filter based on the heat equation with heat source, availability of coarse and precise levels of contour approximation, automated snake initiation. The technique is successfully implemented for segmenting cytological specimen images.

ACKNOWLEDGEMENTS

This work is partially supported by Russian Foundation for Basic Research Grants NN 05-07-08000, 06-01-81009, 06-07-89203, by the project within the Program of the Presidium of the Russian Academy of Sciences "Fundamental Problems of Computer Science and Information Technologies", and by INTAS Grant N 04-77-7067.

REFERENCES

Borst, H., Abmayr, W., and Gais, P., 1979. A thresholding method for automatic cell image segmentation*, J. Histochem. Cytochem.,27*(1), pp 180–187.

Belyaev, A.G., Pasko, A.A., KuniiT.L., 1998. Ridges and Ravines on Implicit Surfaces. *Computer Graphics International (CGI '98), June 22-24,* Hannover, Germany, pp. 530-535.

Bengtsson, E., Wahlby, C., Lindblad, J., 2004. Robust Sell Image Segmentation Methods. *Pattern Recognition and Image Analysis. Advances in Mathematical Theory and Applications. Vol.14, No. 2,* pp. 157 – 167.

Caselles, V., Catte, F., Coll, T., Dibos, F. 1993. A geometric model for active contours. *Numerische Mathematik 66*, pp. 1-31.

Comaniciu, D., Meer, P., 2001. Cell Image Segmentation for Diagnostic Pathology, *Advanced Algorithmic Approaches to Medical Image Segmentation: State-Of-The-Art Applications in Cardiology, Neurology, Mammography and Pathology* . J. Suri, S. Singh and K. Setarehdan (Eds.), Springer, pp. 541-558.

Colantonio S., Gurevich I.B. Salvetti O., 2006. Automatic Fuzzy-Neural Based Segmentation of Microscopic Cell Images, *In Workshop Proceedings: Petra Perner (Ed.), Workshop on Mass-Data Analysis of Images and Signals,* MDA 2006 IBaI CD-Report, p. 34-45.

Eberly, D., Gardner, R., Morse, B., Pizer, S., and Scharlach, C., 1994. Ridges for image analysis, *Journal of Mathematical Imaging and Vision, 4, 4, December, pp. 353 – 373.*

Haralick, R. M., Shapiro, L. G., 1985. Image Segmentation Techniques, *Computer Vision, Graphics, and Image Processing, 29, 1*, pp. 100-132.

Kass, M., Witkin, A., Terzopoulos, D. 1987. Snakes: Active contour models. *Int. Journal on Computer Vision, 1,* pp. 321-331.

Koederink, J., 1984. The structure of images. *Bio. Cybern., 50,* pp.363 - 370.

Klemencic, A., Kovacic, S., Pernus, F., 1998. Automated segmentation of muscul fiber images using active contour models*, Cytometry 32*, pp. 317-326.

Soille, P., 2004. *Morphological Image Analysis: Principles and Applications,* Springer-Verlag, Berlin.

Lindeberg, T., 1994. *Scale-space Theory in Computer Vision.* Kluwer Academic Publishers.

Lee, E.B., Markus, L., 1971. *Foundations of optimal control theory,* J. Willey & Sons, Inc., New York, London, Sydney.

Leymarie, F., 1990. Tracking and Describing Deformable Objects Using Active Contour Models. *Technical Report CIM-90-9,* McGill Research Center for Intelligent Machines, 186 p.

Malpica, N., Ortiz de Solorzano, C., Vaquero, J.J., et. al., 1997. Applying watershed algorithms to the segmentation of clustered nuclei. *Cytometry. 28*, pp. 289-297.

Ortiz de Solorzano, C., Malladi, R., Lelievre, S.A., Lockett,S.J., 2001. Segmentation of nuclei and cells using membrane related protein markers. *Journal of Microscopy, 201*, pp. 404-415.

Rohr, K., 2001. *Landmark-Based Image Analysis Using Geometric and Intensity Models*, Kluwer Academic Publishers, 303 p.

Pratt, W.K. 2001. *Digital Image Processing: PIKS Inside*, John Wiley & Sons, Inc., 735 p.

Sapiro, G., 2001. *Geometric Partial Differential Equations and Image Analysis*.Cambridge University Press, Cambridge.

Xu, C., Prince, J.L., 1998. Snakes, Shapes, and Gradient Vector Flow. *IEEE Transactions On Image Processing, 7 (3),* pp.359-369.

Yang, L. Meer, P., Foran, D., 2005. Unsupervised segmentation based on robust estimation and color active contour models, *IEEE Trans. on Information Technology in Biomedicine*, 9, pp. 475-486.